Boundary-Layer Meteorol (2013) 146:469–496
DOI 10.1007/s10546-012-9773-y

ARTICLE

Intra-City Variation in Urban Morphology and Turbulence Structure in Helsinki, Finland

Annika Nordbo · Leena Järvi · Sami Haapanala · Joonas Moilanen · Timo Vesala

Received: 9 March 2012 / Accepted: 18 September 2012 / Published online: 11 October 2012

Abstract Most atmospheric boundary-layer theories are developed over vegetative surfaces and their applicability at urban sites is questionable. Here, we study the intra-city variation of turbulence characteristics and the applicability of boundary-layer theory using building-morphology data across Helsinki, and eddy-covariance data from three sites: two in central Helsinki (400 m apart) and one 4 km away from the city centre. The multi-site measurements enable the analysis of the horizontal scales at which quantities that characterize turbulent transport vary: (i) Roughness characteristics vary at a 10-m scale, and morphometric estimation of surface-roughness characteristics is shown to perform better than the often used rule-of-thumb estimates (average departures from the logarithmic wind profile are 14 and 44 %, respectively). (ii) The drag coefficient varies at a 100-m scale, and we provide an updated parametrization of the drag coefficient as a function of z/z_{H} (the ratio of the measurement height to the mean building height). (iii) The transport efficiency of heat, water vapour and CO_2 is shown to be weaker the more heterogeneous the site is, in terms of sources and sinks, and strong scalar dissimilarity is observed at all sites. (iv) Atmospheric stability varies markedly even within 4 km across the city: the median difference in nocturnal sensible heat fluxes between the three sites was over 50 W m^{-2}. Furthermore, (v) normalized power spectra and cospectra do not vary between sites, and they follow roughly the canonical theory as developed over vegetated terrain.

Keywords Drag · Eddy covariance · Roughness · Turbulence · Urban site

1 Introduction

At present, over 70 % of Europeans and over half of the World's population live in cities, and in 2050 the fraction of city dwellers is estimated to reach two thirds of the World's population (United Nations Population Division 2010). Alterations in land use and atmospheric

A. Nordbo (✉) · L. Järvi · S. Haapanala · J. Moilanen · T. Vesala
Department of Physics, University of Helsinki, P.O. Box 48, 00014 Helsinki, Finland
e-mail: annika.nordbo@helsinki.fi

composition caused by urban development has led to the establishment of urban microclimates. These climates differ from their rural counterparts due to differences in the exchange of momentum, heat, gases and particulate matter. Consequently, the understanding of this surface–atmosphere exchange is the key to understanding and predicting urban climates. Furthermore, these efforts benefit city design through e.g. wind-load prediction and human comfort through appropriate city design (e.g. Coutts et al. 2007; Stone et al. 2010).

The eddy-covariance (EC) method is the only direct means of measuring turbulent fluxes. In the urban environment, the method is favoured over flux–gradient methods that, inter alia, require similarity of eddy diffusivity coefficients (Roth and Oke 1995). Nevertheless, the EC method also has its underlying measurement criteria: (i) the atmospheric flow should be stationary (the properties of turbulence are time independent), (ii) the surface should be reasonably horizontally homogeneous, and (iii) the fluxes should be constant with height in the inertial sublayer where the sensors are placed (Munger et al. 2012).

Despite the stringent criteria, there are a growing number of EC measurements in complex, urban environments around the globe (see e.g. Velasco and Roth (2010) for a review on CO_2 fluxes and Nordbo et al. (2012) for a review on energy fluxes). Most studies have concentrated on the surface energy balance or CO_2 fluxes whereas only a few investigate the urban turbulence structure itself (Roth 2000; Al-Jiboori et al. 2002; Moriwaki and Kanda 2006; Hanna and Zhou 2009; Wood et al. 2010). Furthermore, a few groups have performed multisite measurements within a city: Christen and Vogt (2004) had two sites in Basel (Switzerland), 1.5 km apart; Kanda et al. (2006) had five EC towers in Tokyo (Japan) and Weber and Kordowski (2010) present data from two sites in Essen (Germany). Due to the large variability in surface roughness and surface cover between cities, additional measurements are needed to cover the whole urban diversity and therefore to be able accurately to describe and mitigate urban climate effects and to improve urban modelling. The universality of both theoretical and empirical relations should be tested at diverse sites, as was done in the overview by Roth (2000).

The most important theoretical framework in boundary-layer meteorology is perhaps the Monin–Obukhov similarity theory (MOST, also known as surface-layer similarity, Monin and Obukhov 1954), which has later been expanded to cover stable atmospheric stratification. The theory applies in the atmospheric surface layer and most relationships have been developed from data over much less rough, heterogeneous surfaces. In addition to the assumption underlying the EC method, applicability of MOST requires that the influences of surface properties, boundary-layer height and geostrophic winds can be represented through the surface shear stress. These requirements are often not fulfilled in an urban environment, which is characterized by increased and variable roughness in addition to heterogeneity in sources and sinks of heat and mass. Nevertheless, the theory is still often used, for instance in pollutant dispersion modelling (e.g. Sofiev et al. 2010). Especially, research on turbulent flow over rough surfaces in stable atmospheric conditions is scarce.

The surface roughness of a city needs to be determined in order to enable the use of MOST and to compare results between various sites; the two most important variables are the aerodynamic roughness length and zero-plane displacement. Detailed knowledge of these parameters is particularly important in complex environments since they affect turbulence structure and turbulent transport. The parameters can be calculated following two main approaches: the morphological and micrometeorological methods (Grimmond and Oke 1999). In the aerodynamic method, these parameters are calculated based on the logarithmic wind profile, whereas in the morphometric method the calculations are based on the roughness element dimensions. The latter requires a roughness element database and is based on parametrizations (MacDonald et al. 1998), and it is the approach adopted in this study.

We address the need for further study of the surface–atmosphere exchange over rough, urban surfaces—especially in stable situations—by presenting data that cover a full year in the high latitude city of Helsinki in Finland. The data were collected at three sites, from which two are located in the centre (data periods: 7 and 9 months) and one at the University of Helsinki campus 4 km from the city centre (full year). The aim is to study the intra-city variation in urban morphology, in turbulent fluxes and in turbulence structure. The latter will have the main emphasis and will include the analysis of atmospheric stability, the drag coefficient, integral turbulence characteristics and turbulence spectra. This should improve our understanding of the applicability of the EC method and the validity of MOST in urban areas, through the introduction of two new high latitude measurement sites with a very high fraction of impervious surfaces. The sites in Helsinki are characterized by heterogeneous surfaces, the vicinity of the sea and the cold climate, and thus the applicability of the EC method is a special challenge. The results have implications on the grid size in modelling approaches: how large is the intra-city variation in turbulence structure in a particular city and what is the influence on numerical weather prediction and pollutant dispersion modelling. Three horizontal scales of variation can be drawn from the measurements: a quantity is interpreted to vary (i) at the 10-m scale if changes are seen with a few degree difference in wind direction, (ii) at the 100-m scale if differences are seen between the two downtown sites or between sectors at the campus site, and (iii) at the kilometre scale if differences are seen between sites 4 km apart.

2 Methods

2.1 Study Sites and Measurement Set-ups

The measurements were undertaken at three urban sites in Helsinki between July 2010 and June 2011, with a 4-month overlapping period (Table 1). Two of the sites, Fire Station and Hotel Torni, are located 400 m apart at the centre of Helsinki (Fig. 1). The third site, SMEAR III, is located 4 km north-east of the centre (*Station for Measuring Ecosystem-Atmosphere Relationships*, Järvi et al. 2009b). The area around SMEAR III can be divided into three surface cover sectors (built 320–040°, road 040–180° and vegetation 180–320°) designated according to the dominant land use. The Fire Station and Hotel Torni sites, conversely, are both characterized by rough and impervious urban land use in all directions. A heavily trafficked road with 44000 vehicles per workday passes the SMEAR III station in the road sector, whereas the traffic volume downtown is less, around 22,000 vehicles per day (Lilleberg and Hellman 2011). Furthermore, due to the vicinity of the road, the area around SMEAR III has been found to be a large source of CO_2 to the atmosphere (1.8 kg C m^{-2}, Järvi et al. 2012).

Turbulent fluxes of momentum (τ), sensible heat (H), latent heat (LE) and carbon dioxide (F_c) were measured using the EC technique at all sites. The set-ups consisted of a three-dimensional sonic anemometer (USA-1, Metek GmbH, Germany) for acquiring the three wind components and sonic temperature, and infrared gas analyzers (IRGA) for measuring the CO_2 and water vapour concentration fluctuations. SMEAR III had a closed-path (LI-7000, LI-COR Biosciences, Lincoln, NE, USA) and open-path (LI-7500) IRGA, Fire Station an enclosed-path (LI-7200) and open-path IRGA, and an enclosed-path IRGA was used at Hotel Torni. The main analysis in this study is done using the closed-path or enclosed-path analyzers, but a short comparison with the open-path analyzers is given to ensure the data quality (Sect. 3.3.1).

Table 1 Characteristics of the three EC measurement stations

	SMEAR III	Fire Station	Hotel Torni
Measurement setup			
Coordinates (WGS84)	60°12′10.14″N	60°09′54.74″N	60°10′04.09″N
	24°57′40.06″E	24°56′43.37″E	24°56′19.28″E
Mast height (m a.g.l.)	31.0	41.8	60.0
Base altitude (m a.s.l.)	29.0	23.0	15.2
Flow distortion	0–50°	90–180°	50–185°
Sonic type	Metek USA-1	Metek USA-1	Metek USA-1
IRGA type	Closed- and open-path[a]	Enclosed- and open-path	Enclosed-path
Tube material	Stainless steel	Stainless steel	Bev-a-line
Tube length (m)	40	2.0	1.9
Tube diameter (mm)	4.0	3.0	3.5
Flow rate (lpm)	17.0	15.1	11.0
Reynolds number	3000	3600	2200
Tube heating (W m^{-1})	16	9[b]	7[c]
Inlet filter type	Gelman Acro 50	Whatman HEPA-CAP 36	No filter
Measurement period	1.12.2005	28.6.2010–27.1.2011	28.9.2010
Measurement period in this study	1.7.2010–30.6.2011	1.7.2010–27.1.2011	28.9.2010–30.6.2011
Urban canopy zone (Oke 2006)	6	2	2

	Built	Road	Vegetation		
Roughness characteristics					
Building height, z_H (m)	20 ± 2	–	–	21.7 ± 3.6	24.1 ± 4.9
Plan area fraction, λ_p	–	–	–	0.40 ± 0.07	0.37 ± 0.08
Frontal area fraction, λ_f	–	–	–	0.46 ± 0.15	0.44 ± 0.16
Zero-plane displacement height, z_d (m)	13	8	6	14.4 ± 3.2	14.9 ± 3.0
Aerodynamic roughness length, z_0 (m)	2	–	–	1.2 ± 0.3	1.4 ± 0.5
Drag coefficient, C_D (10^{-2})	2.73 ± 1.08	1.64 ± 0.77	1.50 ± 0.64	1.72 ± 1.09	1.54 ± 0.90
Surface cover					
Built	0.43 ± 0.04	0.31 ± 0.11	0.12 ± 0.12	0.57 ± 0.11	0.55 ± 0.14
Paved	0.15 ± 0.02	0.32 ± 0.08	0.21 ± 0.13	0.35 ± 0.09	0.42 ± 0.13
Unmanaged	0.00 ± 0.00	0.03 ± 0.06	0.00 ± 0.00	0.02 ± 0.05	0.01 ± 0.02
Vegetation	0.41 ± 0.04	0.34 ± 0.11	0.66 ± 0.08	0.05 ± 0.07	0.02 ± 0.03
Water	0.00 ± 0.00	0.00 ± 0.00	0.01 ± 0.01	0.01 ± 0.04	0.00 ± 0.00

SMEAR III station is located 4 km from the centre of Helsinki and it is characterized by a high vegetation fraction; Fire Station and Hotel Torni stations are located downtown, about 400 m apart. Roughness characteristics, surface cover and drag coefficient: values are given for three sectors at SMEAR III; values for z_H, z_d and z_0 at SMEAR III are from Vesala et al. (2008b); all other values are given as means ($\pm$ standard deviation with wind direction) and are for a 500-m circle around the tower. Only data from wind directions without flow distortion are included in the calculation of the means and standard deviations. The drag coefficients are calculated from EC measurements in neutral atmospheric conditions ($|\zeta| < 0.01$)

[a] The open-path IRGA was not functioning between mid-December and mid-April

[b] Installed 23 Nov 2010

[c] Installed 4 Nov 2010

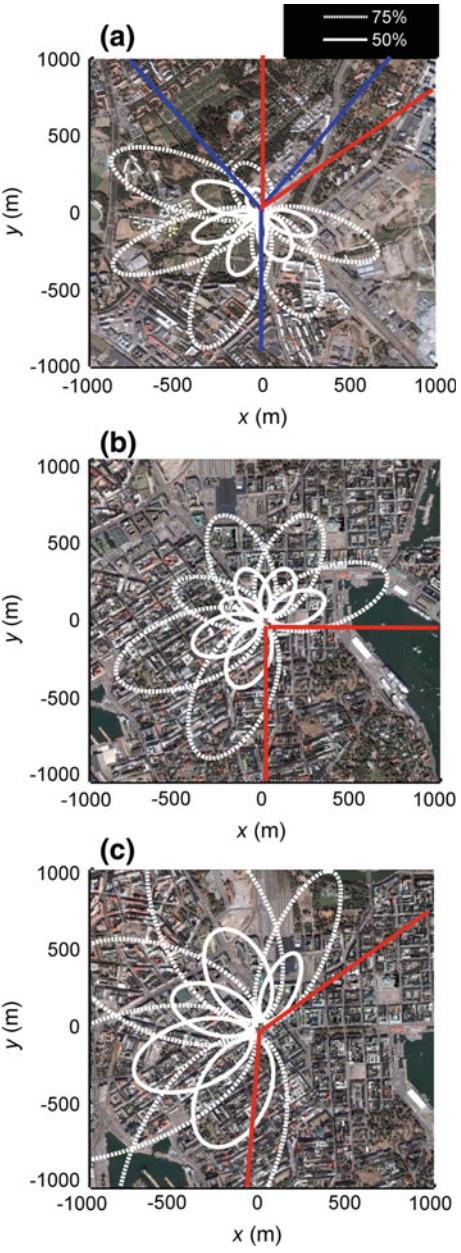

Fig. 1 Maps of measurement sites: **a** SMEAR III, **b** Fire Station and **c** Hotel Torni. Footprint isopleths (contours of areas that contribute to the measured flux: 50 % *continuous*, 75 % *dashed*) are superimposed on Google Earth maps for a 2×2 km^2 area around the stations. The isopleths are calculated for 45° wind direction sectors with mean conditions for a chosen stability class ($\zeta = -0.05$ for SMEAR III and $\zeta = -0.1$ for Fire Station and Hotel Torni). The mean conditions are calculated from data for the whole measurement period (Table 1). Wind directions with flow distortion are marked with *red lines* and three diverse wind direction sectors of SMEAR III are marked with *blue lines*

The EC equipment was mounted on small masts on towers at the downtown sites (Fig. 2), whereas measurements were performed on a lattice tower at SMEAR III (Vesala et al. 2008b). At Fire Station, a 3.8-m high mast was mounted on the north-west corner of the fire station tower (Fig. 2b); at Hotel Torni, a 2.3-m high mast was installed on the north-west corner of the tower of the hotel (Fig. 2e). Flow towards the equipment on both masts is obscured

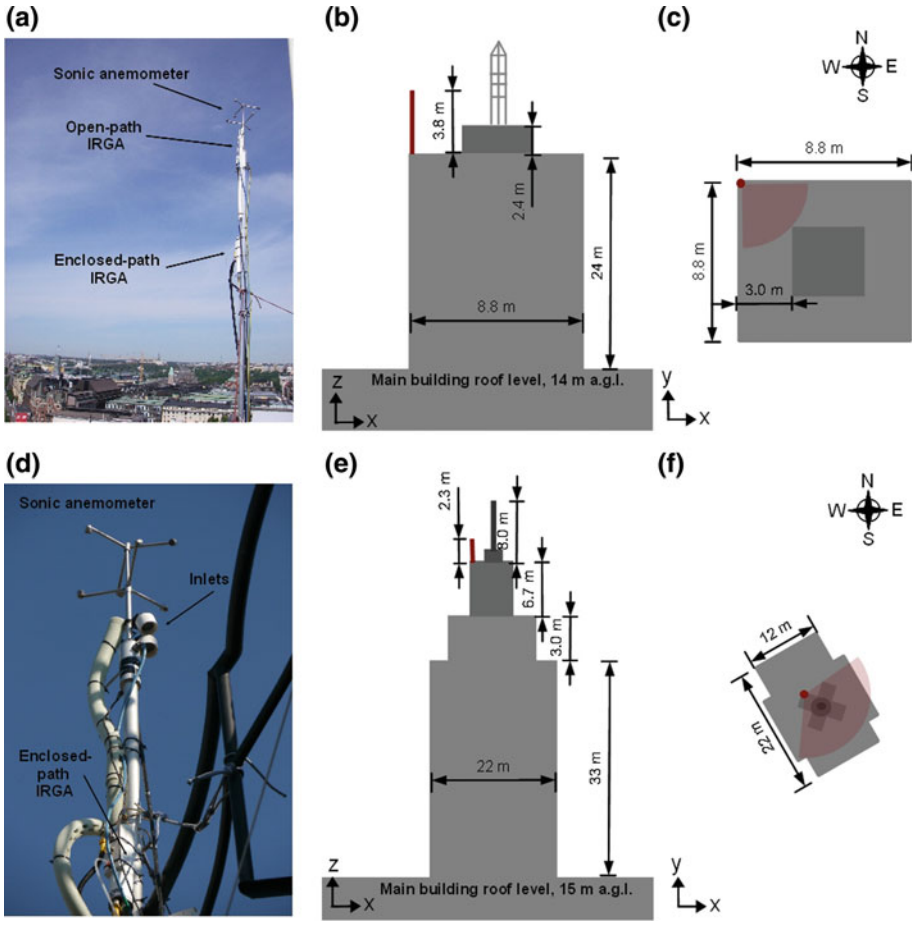

Fig. 2 Photographs and schematics of Fire Station (**a**–**c**) and Hotel Torni (**d**–**f**). Photo in (**a**) is taken facing north and measurement equipment are shown with arrows. Photo in (**d**) is taken from below and the *black rail* in the photo is horizontal although it might not appear so. Frames (**b**) and (**e**) are vertical cross-sections of towers on the main buildings. Frames (**c**) and (**f**) are plan views of the buildings and sectors with flow distortion are shown with translucent *red areas* (see Sect. 2.3 for further details). The measurement masts are shown in *red* in (**b**), (**c**), (**d**) and (**f**). Note that schematics of each site are in approximate scale, but the schematics are not in scale between sites

by structures in the centre of the towers (translucent red sectors in Fig. 2c, f; discussed in Sect. 2.3).

EC measurements were accompanied by auxiliary meteorological measurements, with equipment installed on the rooftop of a university building (24 m a.g.l., 51 m a.s.l.), 100 m north-east from the SMEAR III tower where the EC measurements were made. The set includes measurements of air temperature (platinum resistant thermometer, Pt-100), air pressure (silicon aneroid barometer, Vaisala DPA500, Vaisala Oyj, Vantaa, Finland), relative humidity (*RH*, platinum resistance thermometer and thin film polymer sensor, Vaisala HMP243), and precipitation (raingauge, Pluvio2, Ott Messtechnik GmbH, Germany). Data were divided into seasons based on a thermal method according to the 5-day running mean air

temperature: spring and autumn are periods where the temperature is between 0 and 10 °C, and winter and summer have temperatures below 0 °C and over 10 °C, respectively.

The Helsinki metropolitan area comprises an area of 765 km^2 and has a population slightly exceeding one million. It is situated on the shore of the Gulf of Finland with weather varying from marine to continental, depending on the origin of the prevailing air mass. The mild northern Atlantic Ocean (and North Atlantic Drift) ensures a milder winter than is to be expected based solely on the high latitude. The northern location has, though, an important role in the varying sun-lit hours, which range from 6 to 19 h per day. The monthly mean temperatures vary from −4.9 °C in February to 17.2 °C in July, and the mean yearly cumulative precipitation amount is 642 mm (1971–2000, Drebs et al. 2002).

2.2 Surface Cover and Morphology

The zero-plane displacement (z_d) and aerodynamic roughness length (z_0) are important variables describing the aerodynamic roughness of the area surrounding the measurement towers. Each was calculated for the Fire Station and Hotel Torni sites following a morphometric method (MacDonald et al. 1998), which is shown to perform well for sites similar to ours (Grimmond and Oke 1999). The calculations were done for a circular area around the sites, using 20°-wide sectors, with a 1° step. The circle radius was varied from 500 to 1,000 m, with a 100-m resolution.

The displacement height is assumed to be solely a function of building height (z_H) and plan area fraction (λ_p, the land fraction that is covered by buildings). The roughness length, however, is dependent also on the frontal area fraction (λ_f) of the buildings. For the calculation of this fraction, the area around a measurement station was divided into four inflow sectors (north, east, south, west) to take into account the flow direction at the tower. Only the walls that are facing the inflow direction were taken into account in the calculation of the frontal area fraction. A projection normal to the wind direction is calculated for the walls that are at an angle to the incoming flow. The stability dependency of z_0 and z_d (Zilitinkevich et al. 2008) was not taken into account, due to the lack of appropriate morphologic parametrizations for urban surfaces.

Land-cover data were divided into five classes: built, paved, unmanaged, vegetation and water and the fraction of each cover was also calculated for a circular area with a radius ranging from 500 to 1,000 m, with a 100-m resolution. Data on land cover and building characteristics were provided by the Helsinki Region Environmental Services Authority (HSY 2008), while land-cover data have a spatial resolution of 10 m, and building data have a 1-m resolution.

2.3 Eddy-Covariance Calculations

Raw EC data were logged at 10 Hz for post processing, and fluxes were calculated with 30-min averaging according to widely-accepted calculation procedures (Aubinet et al. 2000). A two-dimensional coordinate rotation was applied to wind-speed data, all data were linearly detrended, and the time lag between wind speed and scalar data was taken into account by maximization of the cross-correlation function. Furthermore, a density correction (Webb et al. 1980) was applied to open-path IRGA data, H values were corrected for cross-wind effects and sonic heating (Liu et al. 2001), and spectral corrections were applied to all fluxes. After flux calculations, quality screening was applied to flux values to ensure an adequate stationarity in the turbulent signal (Foken and Wichura 1996). In addition, open-path IRGA

data were omitted at times of precipitation, and all flux data were omitted when the wind direction results in flow distortion (Table 1). This flow distortion is due to tower structures and not to other buildings. The sectors affected by flow distortion were determined by visually inspecting the wind-speed spectra and cospectra, and usually resulted in unrealistic drag coefficients (see later). All data from these sectors were omitted. A more detailed description of the calculation procedures is provided elsewhere (Nordbo et al. 2012).

In addition to the data screening in respect to flux stationarity and flow distortion, the detection limit and random uncertainty relative to flux magnitude were calculated. Thorough descriptions are available elsewhere (Nordbo et al. 2012) and a brief description only is given here. The flux detection limit was calculated as the standard deviation of the cross-covariance function away from its maximum (Wienhold et al. 1994). The random flux error was calculated according to Lenschow et al. (1994), as

$$\sigma_{\mathrm{F}}^2(\Gamma) \approx 2\frac{\Gamma_{\mathrm{f}}}{\Gamma}\left(\mu_s\mu_w + \overline{w's'}^2\right), \tag{1}$$

where Γ is the averaging period (30 min), Γ_{f} is the integral time scale, and μ_s and μ_w are the variances of the scalar s and w. The detection limit has units of covariance and the random flux error has units of covariance squared, and thus both can be converted so as to be relative to the observed flux.

The EC measurements allow the calculation of several variables describing turbulence characteristics: (i) the atmospheric stability is defined as $\zeta = (z - z_{\mathrm{d}})/L$, where z is the measurement height and $L = -\frac{\rho_{\mathrm{a}} c_{\mathrm{pa}} u_*^3}{k(g/T)H}$ is the Obukhov length. Here ρ_{a} is air density, c_{pa} is the heat capacity of air at constant pressure, u_* is the friction velocity, k is the von Kármán constant (0.4), g is the gravitational acceleration (9.81 m s^{-2}) and T is air temperature. Five stability categories are used here: very unstable ($\zeta < -1$), unstable ($\zeta < -0.01$), neutral ($-0.01 < \zeta < 0.01$), stable ($\zeta > 0.01$) and very stable ($\zeta > 1$). (ii) The drag coefficient $\left(C_{\mathrm{D}} = (u_*/U)^2\right)$ relates the momentum transfer to the mean wind speed (U) and characterizes the surface aerodynamic roughness. The C_{D} defined here is actually a bulk transfer coefficient deduced from EC measurements and widely used in micrometeorology. It varies with the surface roughness of the source area (see Sect. 2.4) of the measurements, and therefore varies with wind direction when the surface is not uniform around the measurement tower. When measurements are performed in the inertial sublayer, u_* is nearly constant with height. Consequently, the micrometeorological C_{D} introduced here should be distinguished from the object-dependent drag coefficient used in fluid dynamics. (iii) The integral turbulence characteristics (ITC, a.k.a. normalized standard deviations) describe the relationship between standard deviations (σ) and fluxes (covariances). The following parametrizations are in wide use for wind-speed components, temperature and other scalars (Monin and Yaglom 1975; Panofsky et al. 1977)

$$\sigma_{u,v,w}/u_* = C_1(1 + C_2|\zeta|)^{C_3}, \tag{2}$$

$$\sigma_{\mathrm{T}}/T_* = \sigma_{\mathrm{T}}u_* \Big/ \left|\overline{w'T'}\right| = C_1|\zeta|^{C_3}, \tag{3}$$

$$\sigma_x/X_* = \sigma_x u_* \Big/ \left|\overline{w'x'}\right| = C_1(1 + C_2|\zeta|)^{C_3}, \tag{4}$$

where $\overline{w'T'}$ is the kinematic heat flux (covariance), X denotes a scalar (c for CO_2, q for water vapour) and $\overline{w'x'}$ is the covariance between vertical wind speed and the scalar perturbation, and with C_1, C_2, C_3 constants. C_3 has a fixed value when $\zeta < 0$ (1/3 for wind and $-1/3$ for scalars) and is allowed to vary for $\zeta > 0$. Other forms of parametrizations have been suggested (Wyngaard et al. 1971; Tillman 1972), but the form presented here is widely

recommended (Arya 2001). Furthermore, the relative transfer efficiency of two scalars can be described as the ratio of their correlation coefficients, which is a function of the ITC

$$\frac{r_{wx_1}}{r_{wx_2}} = \frac{\sigma_{x_2}/X_{2*}}{\sigma_{x_1}/X_{1*}} \tag{5}$$

for scalars X_1 and X_2. (iv) The power spectra and cospectra are calculated using fast Fourier transforms for each 60-min period (with 2^{15} points), using commonly accepted methods (Stull 1988). Fluxes are also calculated with a 60-min averaging period and quality screening is applied to the spectra accordingly.The spectra are then binned into 76 logarithmically evenly-spaced classes and only conditions with quality-assured fluxes are accepted. Normalized forms of power spectra and cospectra are used: they are multiplied by frequency (f, Hz) and divided by variance (σ^2) or covariance ($\overline{w'x'}$), respectively. The peak frequencies of 60-min spectra (f_m) are gained by making a fit to each spectrum and by thereafter locating the maximum of the fit. The frequencies are then converted to a normalized form, $n_\mathrm{m} = (z - z_\mathrm{d})\, f_\mathrm{m}/U$ and a fit to n_m as a function of stability, $n_\mathrm{m} = \alpha_1\,(1 + \alpha_2 \zeta^{\alpha_3})$, is made for analyzing the location of the energy-containing range in cospectra (Nordbo et al. 2012).

2.4 Footprint Estimation

Flux footprints, i.e. the flux source areas (Vesala et al. 2008a), are estimated using an analytical model (Kormann and Meixner 2001). The footprint function depends on the effective measurement height ($z - z_\mathrm{d}$), mean wind speed, friction velocity, stability and cross-wind standard deviation. Data from all sites are divided into 45° wind sectors and eight stability classes, and mean parameter values and corresponding footprints are then calculated for each dataset. The z_d value is taken as an average of the wind direction sector, and the measurement height is site specific.

The analytical model provides a footprint function that gives the relative contribution of a certain area around the tower to the calculated flux value. This function extends theoretically to infinity, but a more sensible measure, footprint isopleths, can be calculated as the volume integral of a contribution function. The 50 % isopleth, for instance, shows the area from which 50 % of the measured flux originates from. In our case, the footprint isopleths, with 50 and 75 % contributions, are shown for the most typical stability class. Furthermore, all assumptions in the model are not fulfilled at our complex sites, but a footprint model for urban sites, where measurements are made close to heterogeneous roughness elements, does not yet exist. Therefore, the footprints are only used to indicate the mean probable source area of the fluxes rather than used hour-by-hour in the flux analysis.

3 Results and Discussion

3.1 Meteorological Conditions

The average 30-min temperature during the studied year (5.6 ± 11.0 °C) is the same as the 30-year climatological mean (Drebs et al. 2002). The monthly average temperatures ranged from −9.8 °C in February 2011 to +22.0 °C in July 2010 (Fig. 3a), and summer and winter were long (40 and 36 % occurrence) whereas spring and autumn were shorter (9 and 14 %). The winter had 139 snow-covered days (Fig. 3a). The mean 30-min wind speed at the 31-m level was 3.4 ± 1.6 m s^{-1} and the cold February had the lowest monthly mean winds, 3.0 m s^{-1}. The dominant wind direction, out of eight classes, was south-west with 22 %

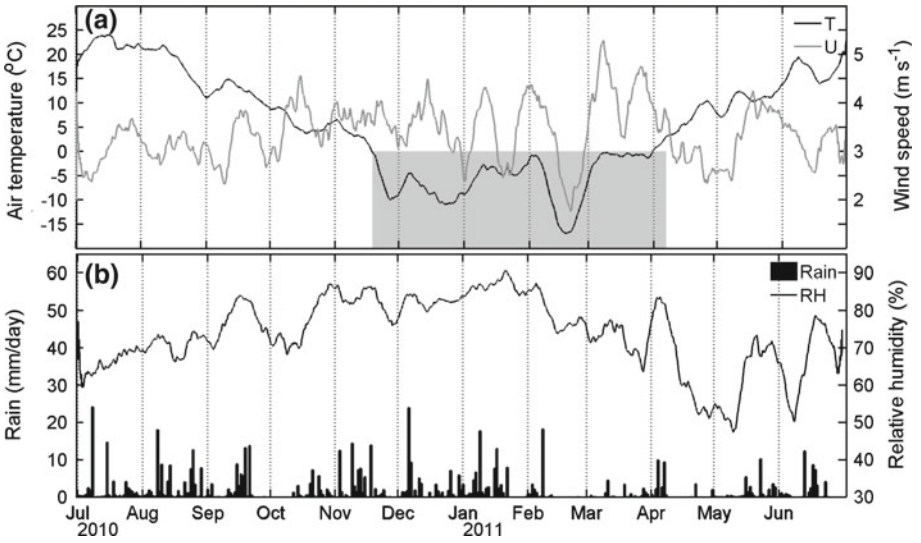

Fig. 3 Meteorological conditions in SMEAR III, Helsinki, from July 2010 to June 2011. **a** Air temperature (T, °C, *left*) and wind speed (U, m s^{-1}, *right*) at 31-m height in addition to the time with snow cover shown as a *grey patch*. **b** Daily precipitation (mm day^{-1}, *left*) and relative humidity (RH, %, *right*). All except precipitation are 5-day running means of 30-min data

occurrence, though there was a large variation between months. Evidence of a sea breeze was observed at all sites in spring since the wind direction tended to change from the sea in the afternoon, as in Järvi et al. (2009b). Furthermore, the average 30-min relative humidity was 4 % lower than the climatological mean, 74 ± 16 %, and the annual precipitation sum was 637 mm, which is only 3 % greater than the climatological mean (Fig. 3b). The precipitation is fairly evenly distributed around the year, with 35 % attributed to snow.

3.2 Source-Area Estimation and Surface Characteristics

The flux footprints are shown in Fig. 1 for weakly-unstable stratification ($\zeta = -0.05$ for the SMEAR III station; $\zeta = -0.1$ for Fire Station and Hotel Torni). The stabilities were chosen based upon the most common stability classes (Fig. 6). The calculations were done using mean parameter values per each 45° wind direction sector. At least half of the flux at the SMEAR III station originates always from a distance less than 500 m from the tower. The footprints depend slightly on wind direction due to variations in d, z_0, U and u_* (in addition to stability), and the footprint is the shortest in the built sector due to a greater aerodynamic roughness. The footprints for SMEAR III have also been calculated previously for neutral stratification with the numerical atmospheric boundary-layer model SCADIS that is based on a 1.5-order turbulence closure (Vesala et al. 2008b). Also at Fire Station, at least half of the flux derives from a circular area with a 500-m radius. The corresponding source area around Hotel Torni is slightly bigger (800-m radius) since the measurements are made at a higher level. The footprints are only indicative of the true source area, and the roughness characteristics around the stations downtown are fairly independent of the distance from the tower (shown later, Fig. 4). Thus, in the following, the surface characteristics are given, for consistency, for a 500-m radius circle around all stations.

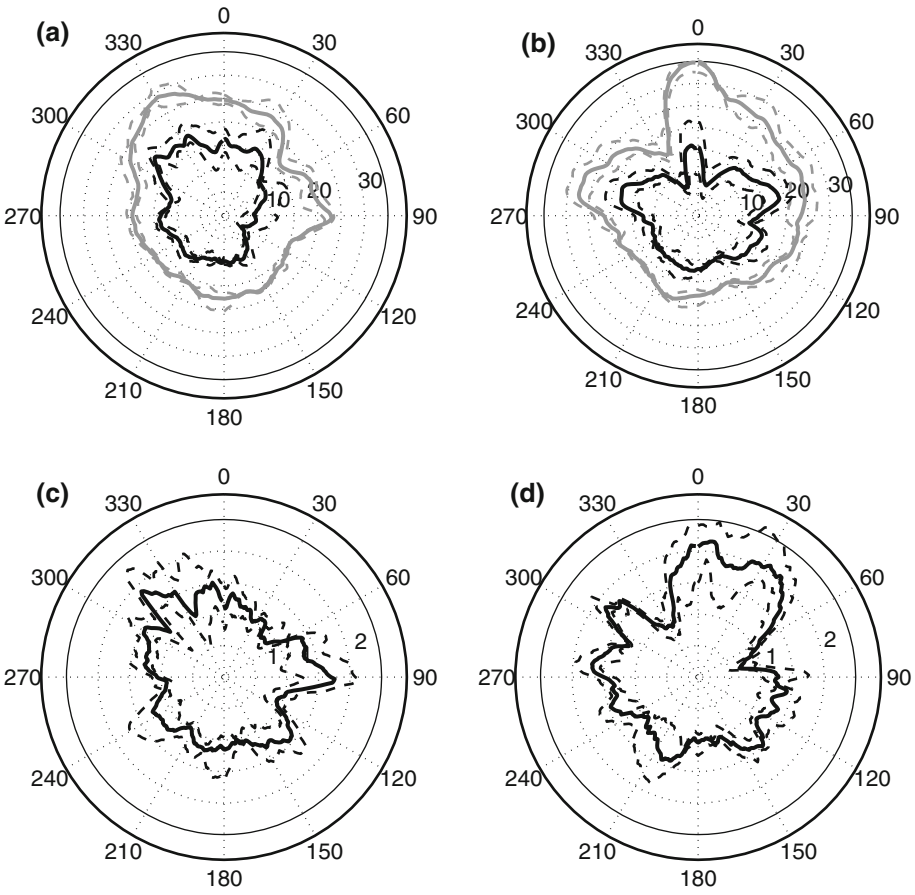

Fig. 4 *Upper figures* show the zero-plane displacement (m, *black*) and building height (m, *grey*) as a function of wind direction for, **a** Fire Station, and **b** Hotel Torni. *Lower figures* show the aerodynamic roughness length (m) as a function of wind direction for, **c** Fire Station, and **d** Hotel Torni. *Dashed lines* are the minima and maxima when varying the radius of the area of interest from 500 to 1,000 m, and the *thick line* is the mean between 500 and 1,000 m

The micrometeorologically-relevant surface aerodynamic roughness estimates and land-cover-fraction estimates for the sites are given in Table 1. The Fire Station measurements are performed 1.8 m below and the Hotel Torni measurements 8.3 m above the recommended height ($z_{\mathrm{min}} = z_{\mathrm{d}} + 4(z_{\mathrm{H}} - z_{\mathrm{d}})$, Foken et al. 2012, p. 31). Furthermore, the Fire Station measurement height is almost twice the mean building height (z_{H}) whereas the Hotel Torni measurements are performed at $2.5z_{\mathrm{H}}$. According to these relations, the instruments at the downtown sites should be at the top of or just above the roughness sublayer (Raupach 1979), which is often considered to extend from a height of $1.5z_{\mathrm{H}}$ in densely built areas to over $4z_{\mathrm{H}}$ in sparsely built areas (Grimmond and Oke 1999). The centre of Helsinki is, indeed, fairly densely built, and λ_{p} is about 0.4 for both sites. The measurements at the SMEAR III site, conversely, are likely performed in the roughness sublayer ($z = 1.55z_{\mathrm{H}}$) when flow is from the built sector. This wind direction is rare (8 % occurrence) and the sector is treated mostly separately in the analysis. Anyhow, the results concerning this sector should be treated

with caution since turbulence might be produced by individual buildings in the roughness sublayer.

The low plan-area fraction downtown indicates that a skimming flow can develop over the buildings: this reduces the rate at which the displacement height grows with λ_p. The displacement heights from morphological parametrizations are about $0.66z_H$ and $0.62z_H$ for Fire Station and Hotel Torni, respectively (Table 1), in accordance with the 'rule-of-thumb' of $0.67z_H$ (Garratt 1992). The roughness length is also a function of λ_f, which is quite high for both sites, around 0.45, and has its maximum at $\lambda_f = 0.19$ and decreases beyond that slowly as λ_f grows (MacDonald et al. 1998). As a result, z_0 for both sites is quite low, about $0.06z_H$, which is lower than the 'rule-of-thumb' of $0.1z_H$ (Garratt 1992).

The aerodynamic roughness parameters depend on the flow direction: for the Fire Station, the mean z_H varies from 15 m (north-east) to 29 m (north–north-west), whereas for Hotel Torni the variation is from 7 m (north–north-west) to 35 m (north) (Fig. 4a, b). The pattern of z_d follows roughly that of z_H—though z_d is also a function of the plan area fraction. The range of z_0 is from 0.8 m (north-east) to 1.9 m (north-west) at Fire Station, whereas the variation at Hotel Torni is from 0.7 m (east) to 2.2 m (north) (Fig. 4c, d). The mean of the values calculated for 500–1,000 m depart slightly from the values gained for a circle with a 500-m radius (7, 15 and 21 % for z_H, z_d and z_0, respectively). To conclude, the roughness parameters are not uniform in all directions, but are fairly insensitive to the radius of the area used.

The built and paved fractions cover over 90 % of the land area downtown and the surface cover is similar in all wind directions (Fig. 1). The area around the SMEAR III site is characterized by large variation between sectors: the built fraction ranges from 12 % in the vegetation sector to 43 % in the built sector, and the paved fraction varies from 15 % in the vegetation sector to 32 % in the built sector. Consequently, vegetation forms a large area around SMEAR III (34–66 %) whereas vegetation is scarce downtown (<5 %). The built fraction downtown departs from λ_p due to the difference in the database resolution: λ_p is calculated from a database with a 1-m resolution and courtyards included, whereas the built fraction is from a database with a 10-m resolution and courtyards are often not resolved. Furthermore, water and unmanaged land have a negligibly small fraction at all sites.

The surface-cover fractions vary with the area of concern: the average of the values calculated for circles ranging from 500 to 1,000 m departs slightly from the value for a 500-m circle. The largest departures are seen for the built fraction at all sites. The least variation is observed at Hotel Torni and Fire Station sites (maximum difference 0.06), and the surface cover around the SMEAR III site varies more as a function of distance from the tower (maximum difference is 0.14). To conclude, the surface-cover fractions downtown are insensitive to the changes in the distance of the footprint maximum, whereas the fractions around SMEAR III are more sensitive.

3.3 Turbulent Fluxes

3.3.1 Eddy-Covariance Data Quality

The EC data quality was ensured by filtering out data that are contaminated by flow distortion and by ensuring flux stationarity. The wind direction criteria produced the rejection of 14.5, 17.0 and 30.5 % of data at SMEAR III, Fire Station and Hotel Tower sites respectively. From the remaining data, 12–45 % were omitted due to low turbulence stationarity, depending on the site and the flux of concern (Table 2). Momentum and CO_2 fluxes appear to be the most stationary whereas water vapour fluxes are quite non-stationary. The Fire Station site has

Table 2 Rejection percentages of data due to low turbulent stationarity, detection limit and random uncertainty

	τ	H	LE	F_c
Data rejection (%)				
SMEAR III	19	34	29	18
Fire Station	23	22	45	23
Hotel Torni	12	29	35	14
Detection limit (%)				
SMEAR III	14	14	13	16
Fire Station	11	12	15	15
Hotel Torni	10	12	13	13
Random uncertainty (%)				
SMEAR III	17	13	17	21
Fire Station	14	12	18	20
Hotel Torni	14	13	16	18

The latter two are given as relative to the flux values. Values are given for momentum (τ), sensible heat (H), latent heat (LE) and CO_2 flux (F_c). Values are for the whole measurement period in this study (Table 1)

the lowest overall data quality. All in all, the number of 30-min periods where flux data remain within the 1-year period is 14,043, 7,955, 7,986 for SMEAR III, Fire Station and Hotel Torni sites respectively. These values correspond to 80, 77 and 60 % of the time when measurements were made, respectively.

Urban sites often have problems with flow deflection associated with buildings (e.g. Barlow et al. 2011). At all our stations, the vertical deflection angle, which sets $w = 0$ in the two-dimensional coordinate rotation ($\sin^{-1}(w/U)$), departs from zero: the average is small at SMEAR III (3.0°, also in Vesala et al. 2008b) but larger for Fire Station (11°) and for Hotel Torni (13°). The non-zero upward vertical deflection might be caused by the towers on which the measurement masts are mounted at the downtown sites. For comparison, Barlow et al. (2011) found that the angle saturates to 6–8° for high wind speeds at the BT tower in London. The deflection at our site should not be a problem for our model of anemometer since the angle of attack still remains within the recommended limits of ±45° (Metek 2006). Barlow et al. (2011) found only a 2 % change in wind-speed statistical quantities when applying a correction based on wind-tunnel experiments in their similar case. Therefore, the flow interference by the towers at our sites is not considered to be severe.

The EC calculation steps have an important effect on the final flux values (e.g. Nordbo et al. 2012). The flux-averaging period of 30 min is appropriate since all fluxes are on average within 1 % of the flux calculated using a 60-min averaging time and within 5 % of the 10-min based flux. Moreover, the fluxes were corrected for spectral loss and the underestimation was about 4 % for τ and 3 % for H, whereas open-path gas fluxes are underestimated by about 5 % and closed-path F_c by 6 %. The closed-path LE has the most severe underestimation, >30 % at all sites, due to sorption effects in tubing and filters. Though the enclosed-path analyzers at Fire Station and Hotel Torni sites had short tubes (Table 1), the attenuation was large due to the dirtying of tubes, insufficient heating and a slow flow rate. Furthermore, the surface heating correction for open-path analyzers was not applied, since it is generally seen as an additional CO_2 uptake.

The enclosed-path IRGA is considered to have the optimal features from both open- and closed-path analyzers (Burba et al. 2010), since closed-path analyzers suffer from large attenuation in tubes (Nordbo et al. 2012; Runkle et al. 2012) and open-path analyzers from surface heating problems (Järvi et al. 2009a). Different analyzers were used in parallel at SMEAR III and Fire Station sites to ensure high data quality. The enclosed-path and

open-path F_c values agreed well at Fire Station ($F_{cOP} = 0.96F_{cCP}$, $r^2 = 0.97$, $rmse = 1.6\,\mu mol\,m^{-2}\,s^{-1}$) whereas LE had greater scatter ($LE_{OP} = 0.89LE_{CP} + 2.96$, $r^2 = 0.85$, $rmse = 7.7\,W\,m^{-2}$). The closed-path and the open-path at the SMEAR III site agreed well for both fluxes ($LE_{OP} = 0.89LE_{CP} + 0.15$, $r^2 = 0.98$, $rmse = 7.3\,W\,m^{-2}$; $F_{cOP} = 0.91F_{cCP} + 0$, $r^2 = 0.91$, $rmse = 2.1\,\mu mol\,m^{-2}\,s^{-1}$). Using short tubes leading to closed- or enclosed-path analyzers is especially important in the urban environment where air pollution is likely to dirty the tube and thus cause larger water vapour flux losses due to tube attenuation. Nevertheless, the closed-path and enclosed-path analyzers are assumed to perform better than the open-path analyzers and thus only data from them are shown in the following.

The relative detection limit and random uncertainty of all fluxes and for all sites are given in Table 2. The detection limit is below 20 % of the measured flux at all sites, implying that the measurement systems are sensitive enough to detect the surface–atmosphere exchange at the sites. The SMEAR III site has the highest relative detection limits of τ, H and F_c but the lowest limits for LE. The discrepancy is caused by the general flux magnitude: evapotranspiration is largest at SMEAR III and thus the measurements are done well above the detection limit. The random uncertainty behaves similarly: the lowest uncertainty in LE is observed at the SMEAR III site, whereas the lowest uncertainty in τ, H and F_c is seen downtown. Generally, the random flux uncertainty is lowest for H (12.6 %, mean of all sites) and highest for F_c (20.3 %).

3.3.2 Temporal Variation of Fluxes and Atmospheric Stability

The temporal dynamics of the surface–atmosphere exchange is analyzed in terms of diurnal cycles. The median diurnal courses of turbulent fluxes, for the 4-month period with data from all sites, are shown in Fig. 5. At all sites, τ values are within the quartiles of the other sites and the flux is mainly governed by the variation in wind speed and surface roughness. H is larger downtown than at the SMEAR III site throughout the year (not shown); for the 4 months of simultaneous measurements from all sites, $H > 0$ at all times and sites, except for nights in October and November at SMEAR III when the flux is directed downward (Fig. 5). The positive nocturnal H is larger downtown (median diurnal course values up to $50\,W\,m^{-2}$), more so for colder months, indicating the existence of an anthropogenic heat source. The Bowen ratio (H/LE) is smallest at SMEAR III with the highest vegetation fraction, and the values from all sites follow the general trend as a function of vegetation fraction (Grimmond et al. 2002). Formation of dew ($LE < 0$) is observed less than 5 % of the time at all sites. Here only data for which the flux exceeds its detection limit are taken into consideration. All fluxes are statistically different between sites ($p = 0.05$), except for the H at Fire Station and Hotel Torni ($p = 0.23$).

F_c downtown and in the road sector of the SMEAR III site are within each other's quartiles. F_c has high values from 0700 to 1800 (local time) at SMEAR III, whereas a clearer peak around 1400 is seen downtown. This is logical since the centre of Helsinki has a steady traffic rate throughout the day and congestion is easily caused (Lilleberg and Hellman 2011). Larger CO_2 emissions are observed at Hotel Torni (medians reaching $23\,\mu mol\,m^{-2}\,s^{-1}$) due to a fairly busy road that lies north of the station. Furthermore, daytime photosynthesis is seen in the vegetation sector of SMEAR III during summer (not shown, see also Järvi et al. 2009a, 2012), whereas nighttime emissions/respiration is about $4\,\mu mol\,m^{-2}\,s^{-1}$ at all sites, around the year (not shown).

Atmospheric stability is an important variable characterizing pollutant dispersion in an urban environment, and is considered in parametrizations of wind profiles or turbulent

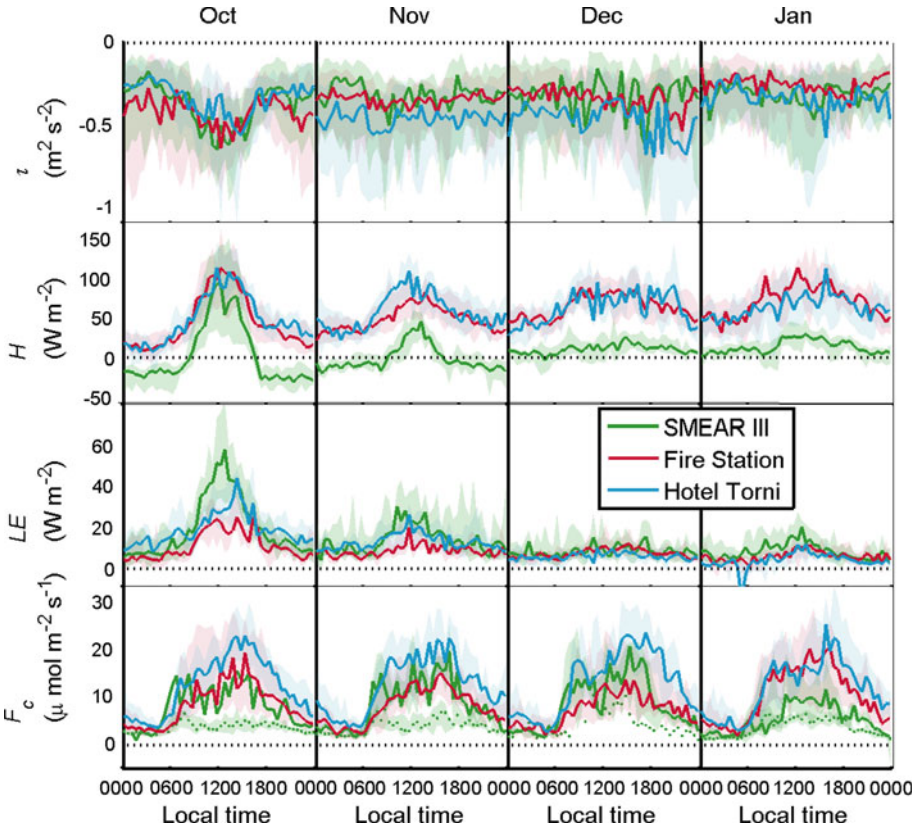

Fig. 5 Median monthly diurnal courses of turbulent fluxes for all three sites for the period when measurements overlap (October 2010–January 2011). Columns are months and rows are fluxes: momentum (τ, $\mathrm{m^2\ s^{-2}}$), sensible heat (H, $\mathrm{W\ m^{-2}}$), latent heat (LE, $\mathrm{W\ m^{-2}}$) and CO_2 flux (F_c, $\mu\mathrm{mol\ m^{-2}\ s^{-1}}$). Patches show 25th and 75th percentiles. Two curves are given for F_c at SMEAR III: flux from the road sector (*solid line*) and from the vegetation sector (*dotted line*). The ground had a snow cover between 18 August 2010 and 6 April 2011

characteristics. Neutral stratification is dominant (73 %) at SMEAR III in Oct–Jan, whereas Fire Station and Hotel Torni are dominated by unstable stratification, 55 and 62 % (Fig. 6). Very unstable stratification is only observed downtown, whereas stable or very stable stratification is common at SMEAR III (15 %) compared with Fire Station (1 %) and Hotel Torni (3 %). The rare stable events downtown are only observed at night, which is in accordance with urban atmospheres tending to be unstable or neutral even at night (Arnfield 2003). Furthermore, less than 1 % of data in Marseille were stable ($\zeta > 0.1$) and unstable stratification was most common ($\zeta < -0.1$, Grimmond et al. 2004). A larger fraction of stable ($\zeta > 0.05$) events was observed at two sites in Essen (19 %, Weber and Kordowski 2010). In contrast, stable stratification prevailed 25 % at 190-m height in London, but the stability parameter is likely to describe surrounding rural surfaces rather than the urban surface due to decoupling of the measurement layer from the surface (Wood et al. 2010).

The intra-city variation in atmospheric stability in Helsinki can be attributed to the variability in the fraction of impervious surfaces and the role of anthropogenic heat release. When evaporation is restricted, the available energy is directed to sensible-heat release that creates

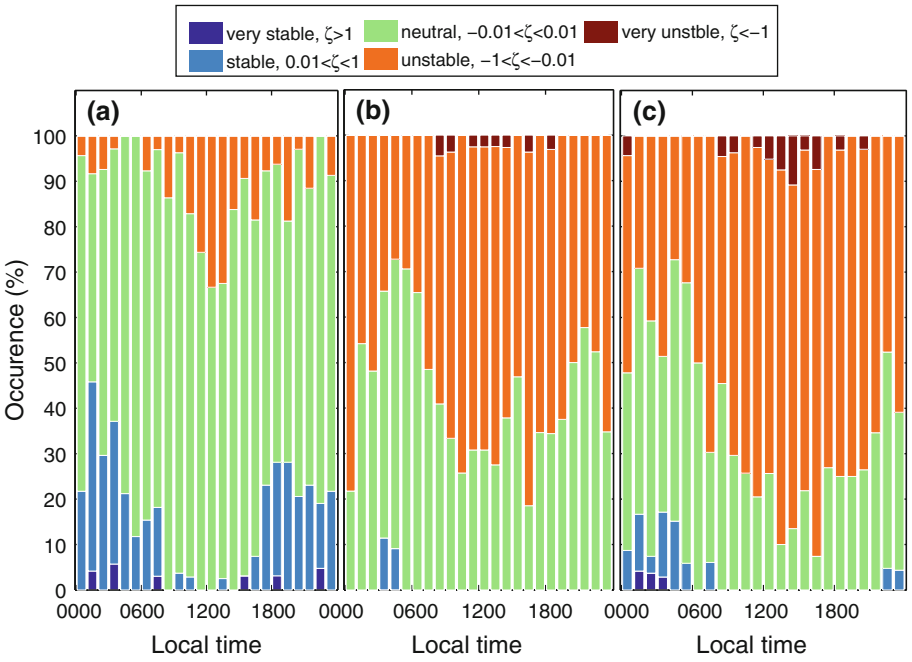

Fig. 6 Relative occurrence (%) of different atmospheric stabilities (ζ) throughout the day at SMEAR III (**a**), Fire Station (**b**) and Hotel Torni (**c**). Only times during which data at all sites are available are included (1,087 data points). The stability classes are shown in the legend

more unstable conditions for areas with lower vegetation fraction. Moreover the high nocturnal H downtown (Fig. 5) is most likely due to anthropogenic heat fluxes or the heat storage flux. Increased surface aerodynamic roughness also increases u_*, this increases L and thus decreases ζ. As a consequence, neither very stable nor very unstable stratification is typically seen over rough surfaces. Furthermore, the more frequent events of stable stratification at Hotel Torni compared with Fire Station might be explained by a 10-m higher measurement level and different footprint: the footprints of the Hotel Torni site extend further away from the core centre to areas where anthropogenic heat release may be smaller.

3.4 Variability in Turbulence Structure

3.4.1 Drag Coefficient

The drag coefficient, $C_\mathrm{D} = (u_*/U)^2$, is important in wind-profile predictions and in parametrizations in numerical weather prediction models. Generally, it increases with surface roughness and decreases with height above the surface. Among our sites, C_D is greatest in the built sector and smallest in the vegetation sector of SMEAR III (Table 1). The average C_D at Hotel Torni is slightly higher than at Fire Stations, as is τ, since $\tau \propto u_*^2$. In the comparison between these sites, the higher roughness overcomes the higher measurement height. At all sites, the probability distribution of C_D has a positive skew.

The values from our sites, in addition to data from recent publications and those reviewed by Roth (2000), are shown for $|\zeta| < 0.05$ in Fig. 7a. Data from our sites are binned to

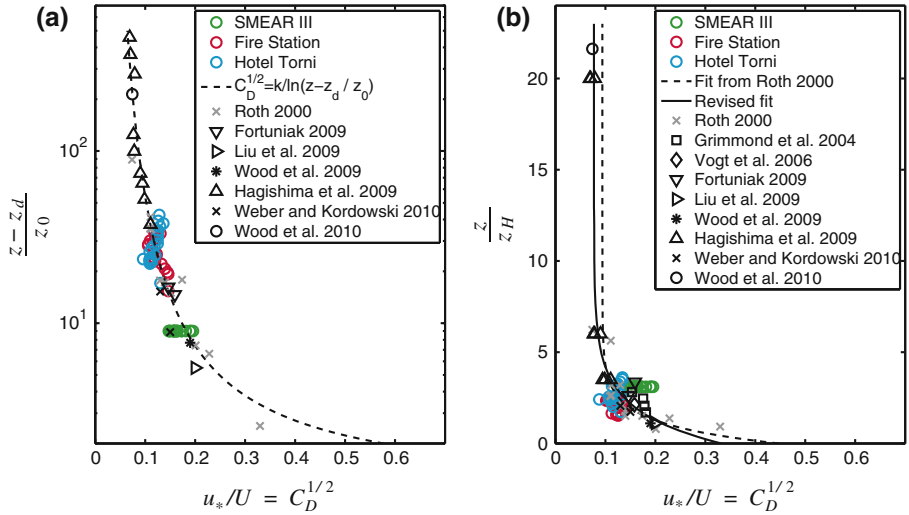

Fig. 7 The variation of, **a** $(z - z_\mathrm{d})/z_0$, and **b** z/z_H as a function of the square root of the drag coefficient ($C_\mathrm{D}^{1/2}$). Data are shown for the built sector of SMEAR III (*green*), Fire Station (*red*) and Hotel Torni (*blue*). Only neutral data ($|\zeta| < 0.05$) are included, and data are binned to 20 classes, each having the same amount of data. Data from recent publications are displayed with *black markers* and data reviewed by Roth (2000) with *grey crosses*. In frame (**a**), the *dashed curve* is according to the logarithmic wind profile. In frame (**b**), the *dashed curve* follows an empirical form by Roth (2000, Eq. 6) and the *solid curve* is a revised fit with all data (Eq. 7). Mean values in neutral conditions, over the whole measurement period for the stations in Helsinki were used in the revised fit: $C_\mathrm{D} = 0.0147, 0.0181, 0.0203$; $(z - z_\mathrm{d})/z_0 = 9.0, 26.0, 33.5$; $z/z_\mathrm{H} = 3.1, 2.1, 2.6$

20 classes, each having the same amount of points. The data collapse on the curve predicted by the logarithmic wind profile (14 % departure, normalized *rmse*), which indicates that the parametrized calculations of z_d and z_0 have been successful. If the rule-of-thumb values for z_0 and z_d (Sect. 3.2) were used downtown, the data points would depart 44 % from the curve. Furthermore, our C_D values downtown are lower than values at the 40 m height in Łódź (Fortuniak 2009, see also Fig. 7), and the results for SMEAR III coincide with one of the sites in Essen (Weber and Kordowski 2010). Fairly high C_D values are observed in Nanjing (22 m height, Liu et al. 2009) and at a rooftop in London (18 m, Wood et al. 2009), where measurements were performed close to the roughness elements. Furthermore, very low C_D values are observed at 190 m height in London (Wood et al. 2010), and Hagishima et al. 2009 give a large range for their wind-tunnel experiments. It must be noted that z_0 and z_d at some sites have been calculated using the logarithmic wind profile and thus the data from these sites join the curve exactly. For our sites, the roughness parameters were determined independent of the logarithmic wind profile, using morphological methods.

Roth (2000) provides a useful framework where data from multiple sites can be compared by expressing the measurement height relative to the mean building height. He gives an empirical curve for the drag coefficient as a function of z/z_H (Eq. 5 in Roth 2000)

$$C_\mathrm{D}^{1/2} = 0.094 + 0.353 \exp\left(-0.946 z/z_\mathrm{H}\right). \tag{6}$$

We provide an updated form of this expression with data extracted from eight new publications and our results (including data in Roth 2000).

$$C_{\mathrm{D}}^{1/2} = 0.0770(0.0583 - 0.0957) + 0.255(0.190 - 0.320)\exp\left(-0.573(0.362 - 0.783)z/z_{\mathrm{H}}\right), \quad (7)$$

where the 90 % confidence intervals are in brackets (see also Fig. 7b). In addition to sites also in Fig. 7a, the fit includes the average value for data from four heights in Marseille (Grimmond et al. 2004) and Basel (Vogt et al. 2006). The original expression is out of the range of the revised expression's confidence intervals. The new data with high z/z_{H} have especially improved this parametrization. It must be noted, though, that parametrizing C_{D} only using z/z_{H} is imperfect since C_{D} depends also on building height, λ_{p} and the direction of flow relative to obstacles (Hagishima et al. 2009). Nevertheless, this empirical curve is a powerful initial approximation for use in parametrizations.

3.4.2 Integral Turbulence Characteristics and Transport Efficiency

Integral turbulence characteristics (ITC) are used in many dispersion modelling applications. Figure 8 shows ITCs as a function of atmospheric stability, and fitting coefficients are found in Table 3 (in the Appendix). Of the three wind components, σ_w/u_* is described best with a stability-dependent curve for unstable and stable stratification, as also shown by Vesala et al. (2008b) for SMEAR III. The parametrization as a function of ζ fails for σ_u/u_* and σ_v/u_* in unstable stratification. The scatter is due to a potential effect of large eddies and thus scaling the variables with the boundary-layer height, rather than the local Obukhov length, could be more appropriate (Panofsky et al. 1977; van den Hurk and de Bruin 1995). Generally, the ITC for wind speed is lower for rougher surfaces, in agreement with the comparison of our sites in Helsinki and with the other studies: for σ_w/u_* largest values are observed over a pine forest (Rannik 1998) and lower values are observed at 47-m height in Beijing (Quan and Hu 2009) and at 190-m height in London (Wood et al. 2010; Helfter et al. 2011). Also, the vegetation and road sectors at SMEAR III have higher values than Fire Station and Hotel Torni, in agreement with the surface roughness (Table 3 in Appendix). It must be noted, though, that 8 % of the SMEAR III data were acquired from measurement heights in the roughness sublayer (built sector).

The integral turbulence characteristics of scalars behave differently to wind speed. σ_{T}/T_* has a clear stability dependency in all stabilities and values peak at neutral stratification where the variation in temperature is large but the flux itself is limited, $H \approx 0$ at neutral (Fig. 8). The largest values are seen for the roughest surfaces since ITC is directly proportional to u_*. The relations for $\zeta > 0$ are not very clear due to the limited amount of data. Furthermore, H_2O and CO_2 exhibit a dependence on stability at all sites for $\zeta < 0$, but none of the sites show a stability dependency for $\zeta > 0$. Quan and Hu (2009) also conclude for H_2O and CO_2, and Rannik (1998) for temperature and H_2O, that the similarity relationships do not seem to describe well the statistics of the fluctuations in stable conditions. Moreover, our results are close to those for a review of sites with $z/z_{\mathrm{H}} > 2.5$ (Roth 2000), results for H_2O in Vancouver (Roth and Oke 1995) and previous results for CO_2 at SMEAR III (Vesala et al. 2008b).

The integral turbulence characteristics are also used for the estimation of turbulent fluxes. Tillman (1972) first suggested the flux–variance method for estimating turbulent fluxes of sensible and latent heat and the relations have later also been used in the variance method in scintillometry. Concluding from our measurements, MOST applies well for the transfer of scalars in unstable conditions, but the relationships are not well-defined for stable stratification. Katul et al. (1995) studied the flux–variance method above uniform and non-uniform terrain and concluded that the method reproduced the EC-based H well, but not for LE.

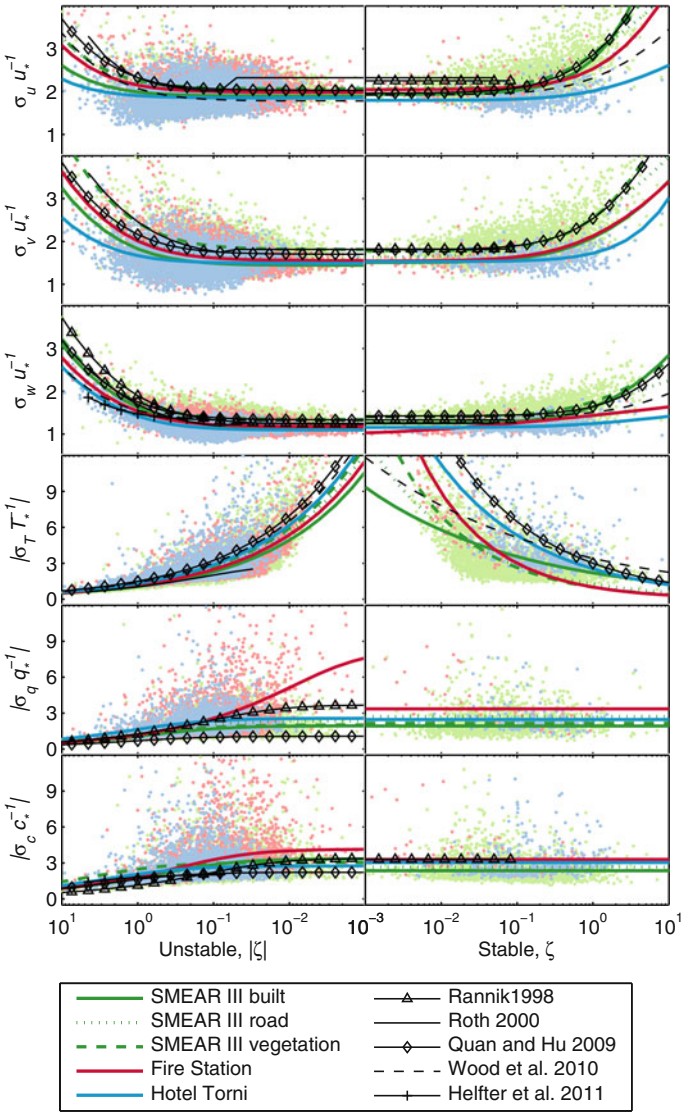

Fig. 8 Integral turbulence characteristics ($|\sigma_x X_*^{-1}|$, Eq. 1–3) as a function of stability (ζ) for unstable (*left column*) and stable (*right column*) situations. X denotes the following variables: horizontal wind (u and v), vertical wind (w), temperature (T), water vapour (q) and carbon dioxide (c). The scalar concentration data are from the closed-path analyzer. Data are from the whole measurement period (Table 1) and shown with light coloured dots for three sectors at SMEAR III (*green*), Fire Station (*red*) and Hotel Torni (*blue*). *Fitted curves* are shown with *darker shades* for all sites and fitting coefficients are given in Table 3 (in the Appendix). *Curves* from recent publications are also displayed for comparison. Rannik (1998) represents a forest site whereas other publications are from urban studies

The integral turbulence characteristics can also be used for the analysis of scalar similarity (Eq. 4). Figure 9 shows the ratio of the sensible heat correlation coefficient to the H_2O and CO_2 flux correlation coefficients as a function of stability, for both unstable and stable

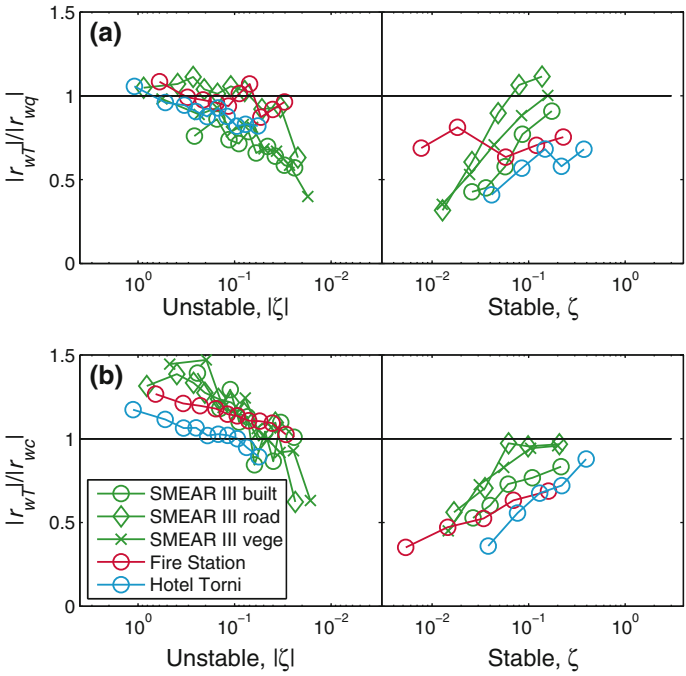

Fig. 9 Ratio of correlation coefficients of sensible heat to H_2O flux (**a**) and sensible heat to CO_2 flux (**b**) as a function of atmospheric stability (ζ). Note that the *x*-axis is logarithmic and data are shown for unstable ($\zeta < 0$) and stable ($\zeta > 0$) situations. Water vapour and CO_2 data are from the closed-path IRGA. Data are medians of values that are binned to 10 unstable classes and 5 stable classes, each having the same amount of data. Data are from the whole measurement period in this study (Table 1) and shown for three wind direction sectors at SMEAR III (*green*) and for Fire Station (*red*) and Hotel Torni (*blue*)

stratification. If MOST applies, the ratios should be unity, which implies that heat and gases are transported by the same turbulence mechanisms. When approaching from unstable to neutral stratification, heat transfer is relatively less efficient at all our sites (Fig. 9, left panels). This may be due to the active role of temperature, whose fluctuations are dynamically related to the actual transport, whereas water vapour and CO_2 are passive scalars. In other words, $\overline{w'T'}$ approaches zero whereas σ_T does not (not shown). This is in accordance with results for water vapour for unstable stratification over vegetative surfaces (Katul et al. 1995; Rannik 1998). To the contrary, at a suburban site in Vancouver, heat transport was always more efficient for $\zeta < -0.05$, and heat transport was observed to become more efficient when approaching neutral stratification (Roth and Oke 1995). The results from Vancouver are consistent with observations at a rural site (McBean 1970). Furthermore, a stability dependency was not observed for H_2O and CO_2 in Tokyo and the ratios for $\zeta < 0$ were on average higher than at our sites, 1.8 and 4.5, respectively (Moriwaki and Kanda 2006). Nevertheless, the observation that H_2O transport is more efficient than that of $CO_2 (r_{wT}/r_{wq} < r_{wT}/r_{wc})$ holds also for our sites for $\zeta < -0.1$.

In stable conditions, the ratios of the correlation coefficients behave similarly: when approaching from stable to neutral stratification, the overall shapes of the curves are mirror images of those for unstable conditions (Fig. 9, right panels). Nonetheless, there is a substantial difference between the behaviour in unstable and stable conditions: the gas transport

is almost always more efficient than heat transport at all our sites in stable conditions. These relationships have not been reported before for stable stratification at urban surroundings. All in all, the ratios in Helsinki depart from unity and a stability dependency is seen for both unstable and stable stratification, which implies dissimilarity in scalar transport. Furthermore, the correlation coefficient between temperature and water vapour approaches zero when water vapour transport is more efficient than heat transport, when approaching neutral from both stable and unstable sides (not shown). This low correlation between temperature and water vapour verifies that the dissimilarity is due to the active role of temperature (Hill 1989; Roth and Oke 1995).

The scalar dissimilarity has intra-city variation. Scalar correlation coefficients exhibit virtually no stability dependency at any of the sites (not shown) and it can be assumed that the stability dependency in Fig. 9 is due to the active role of temperature as a scalar. Thus, the intra-site variability could be attributed to the sparse, heterogeneous distributions of sources and sinks. Weaver (1990) suggests that, when a sparsely-distributed source entrains with the flow, the variance of the gas concentration is increased whereas the covariance is necessarily not. Thus, the correlation coefficient would be reduced compared to an area with a homogeneous source distribution. This is in accordance with the observation that water vapour transport is the weakest downtown and in the road sector of SMEAR III, which is characterized by the highest homogeneity in terms of water vapour sinks and sources. The difference between sectors at SMEAR III is not as pronounced for CO_2. Nevertheless, the transport of CO_2 around Hotel Torni appears to be the most efficient in all stability conditions which corroborates the assumption of the relation between source/sink heterogeneity and transfer efficiency, since Hotel Torni is surrounded by a fairly homogeneous road network. Source/sink heterogeneity was also hypothesized to be the primary reason for the more efficient heat transport in Vancouver and Tokio (Roth and Oke 1995; Moriwaki and Kanda 2006).

3.4.3 Power Spectra and Cospectra

The power spectra and cospectra can be used to evaluate the quality of data and the similarities between scalars. Figure 10 shows the median normalized cospectra and power spectra as a function of normalized frequency (n/n_{m}, with the peak at one). Both velocity power spectra have a well-defined peak that implies that the measurements are performed well above the canopy, and the variance is not due to eddies from element wakes (Roth 2000). The power spectrum of horizontal wind speed follows well the rural reference (Rannik and Vesala 1999) except for lower spectral values around $n/n_{\mathrm{m}} = 0.3$. The low values are not seen for w, but enhanced energy at higher frequencies is apparent. Similar enhanced spectral power was seen in 19 1-h w power spectra from Beijing (Li et al. 2010) and at a forest site (Kaimal and Finnigan 1994, p. 99). All scalar power spectra exhibit enhanced variation at low frequencies that might stem from effects of linear detrending, which cannot remove sub-hour trends. Random noise at the highest frequencies in scalar spectra appears as a rise in the spectra with a slope of unity on a log-log scale. The water vapour and CO_2 fluctuation measurements with a closed-path analyzer are characterized by attenuation in tubes and filters, which can be seen as a too-fast fall at high frequencies.

The loss of variance due to tube attenuation is also evident as a loss of covariance in the cospectra, since the cospectra roll off with a $-7/3$ instead of a $-4/3$ slope. The cospectra of T and w, conversely, do not show much attenuation and follow the rural reference (Kaimal et al. 1972), except for the inertial subrange slope of -1 instead of $-4/3$.

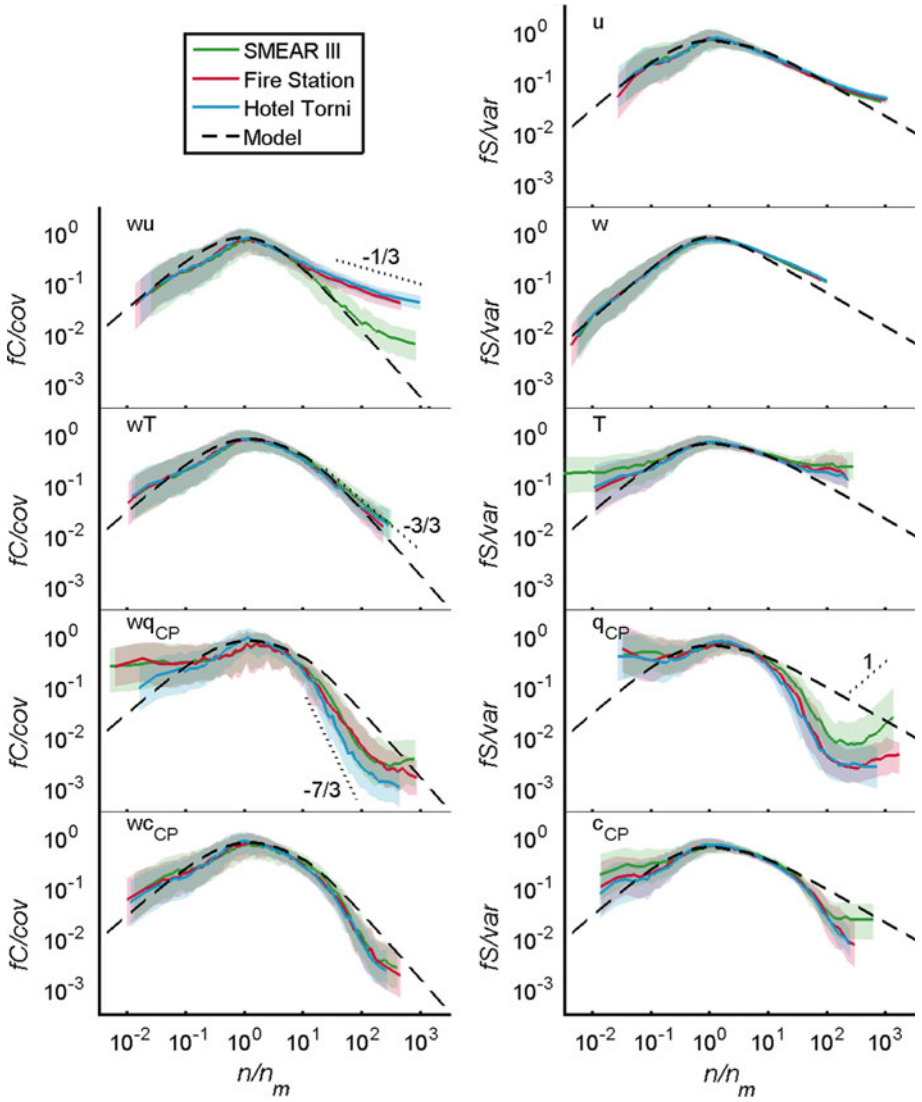

Fig. 10 Median normalized cospectra (*fC*/cov, *left panel*) and power spectra (*fS*/var, *right panel*) as a function of normalized frequency ($n = f(z - z_d)/U$) divided by spectral peak frequency (n_m). Data are from the whole measurement period (Table 1) and binned into 76 classes, each having the same amount of data. Only data for which $\zeta < 0$ are included and the spectra have 290 to 2,687 hours of data, depending on the variable. The shaded areas show the 25 and 75 percentiles. The model curves are for unstable situations, and the cospectra are from Kaimal et al. (1972) and the power spectra from Rannik and Vesala (1999)

Cava and Katul (2012) have observed similar slopes at heterogeneous sites and explain the phenomenon as the effects of surface heterogeneity and scalar dissimilarity.

The momentum cospectrum shows elevated transport at high frequencies, with a slope of –1/3. It is seen at all sites, though it commences at a higher frequency at SMEAR III. All cospectra are distorted from low frequencies to the frequency of the cospectral peak. The location of the distortion is the same as for the u power spectrum. The distortion in

the momentum cospectrum corresponds to a horizontal length scale of about 800 m for Fire Station and of 900 m for Hotel Torni (assuming Taylor's hypothesis of frozen turbulence and using n_m from Table 3 in the Appendix). This length scale is not characteristic of buildings, and the low spectral values might be related to the contrast between the sea and the land. To our knowledge, neither the low cospectral values at low frequencies nor the elevated momentum transport at high frequencies have been reported before. It has been noted, though, that momentum cospectra are often ill-defined in urban environments whereas the cospectrum of T and w often has acceptable behaviour (Roth 2000).

The dependency of the normalized cospectral peak frequency on stability, $n_m(\zeta)$, gives further insight to the size of eddies that cause most of the turbulent transport, i.e. the energy-containing range of the cospectrum. In unstable stratification, all fluxes are produced by larger eddies at SMEAR III compared with Fire Station and Hotel Torni (α_1 in Table 3 in the Appendix). Momentum is transported by larger eddies than is the case for scalar fluxes at all sites, as predicted (Kaimal and Finnigan 1994), but there is variation between n_m for different scalars. The higher n_m for CO_2 compared with water vapour is due to attenuation in tubes in the latter: if flux attenuation starts already close to the cospectral peak, it might appear that the peak is shifted to lower frequencies though in reality it is not. Furthermore, all scalar n_m values are close to a rural reference from a forest ($n_m = 0.09$, Rannik et al. 2004) and are within the range of urban observations of sensible heat transport in unstable stratification (Roth 2000). A stability dependency for $\zeta > 0$ is observed at all sites (not shown) but the fits for the downtown sites suffer from a lack of data in stable stratification. The stability dependency of n_m is not often reported for urban surfaces presumably due to the lack of measurements under stable conditions with a presumed urban source area (rather than for tall tower measurements where the upstream source area might be rural). Our results for CO_2 are in close agreement with previous measurements at SMEAR III (Järvi et al. 2009a).

4 Summary and Conclusions

The EC method was used to measure turbulent fluxes and turbulence characteristics above the roughness sublayer at three urban sites within one city. The data were obtained for 1 year, including a long winter with more than three snow-covered months. The surroundings of two downtown sites (Fire Station and Hotel Torni) are characterized by a high fraction (>90 %) of buildings and impervious surfaces in all wind directions for at least 1 km from the tower (except to the north-east-east at Fire Station). The third site, SMEAR III, is more complex, since the land cover varies greatly with wind direction and distance from the tower. Surface roughness parameters were calculated for the downtown sites using a morphometric approach that takes into account the direction of the flow impacting buildings. The parameters vary with wind direction but are less sensitive to the distance from the tower (Fig. 4). The modified morphometric method was successful in estimating z_0 and z_d since the C_D data collapsed on the curve predicted by the logarithmic wind profile (Fig. 7a). The departure from the curve was 14 %, whereas the usage of rule-of-thumb estimates gave a departure of 44 %. C_D was also shown to have intra-city variation at a scale of some tens to hundreds of metres. Furthermore, a parametrization of C_D as a function of z/z_H was developed using data from over 20 sites and some wind-tunnel experiments (Fig. 7b).

The surface–atmosphere exchange through turbulent fluxes was similar at the two downtown sites, but differed when compared to SMEAR III. This is mostly due to the differences in land cover. H values are larger downtown throughout the day but especially during night: median nocturnal wintertime fluxes reach up to 50 W m^{-2}, which indicates a large

anthropogenic heat source (Fig. 5). Consequently, the atmosphere was mostly unstably stratified ($\zeta < -0.01$) downtown, whereas neutral stratification ($-0.01 < \zeta < 0.01$) prevailed at SMEAR III (Fig. 6). Thus in Helsinki, the stability changes significantly already at the kilometre scale, which would be important to parametrizations in fine-scale dispersion models. In contrast, the heavy trafficked road near SMEAR III had similar F_c values to those observed downtown (diurnal medians exceeding 20 μmol m^{-2} s^{-1}).

The intra-city variation and the validity of MOST was tested using integral turbulence characteristics. The parametrization as a function of ζ fails for σ_u/u_* and σ_v/u_* in unstable stratification, and might be due to the contribution of large-scale eddies. Also, no stability dependency was observed for σ_c/c_* and σ_q/q_* in stable stratification, which has not been shown before for urban sites due to the lack of observations in stable conditions. Furthermore, analysis on relative transfer efficiencies of scalars shows that heat is transferred more efficiently than water vapour and CO_2 in unstable conditions since temperature is an active scalar (Fig. 9). When approaching neutral conditions, heat transfer is relatively weaker at all sites, which has not been observed for urban sites before. The transfer efficiencies also depend clearly on the heterogeneity of the sites: the more heterogeneous the site in terms of sources and sinks, the weaker the transport efficiency. Generally, the assumption of scalar similarity in MOST does not apply at our three sites. Techniques that rely on scalar similarity, such as the Bowen-ratio method, should not be applied in our complex urban environments.

The applicability of theoretical spectral shapes developed at rural sites was also tested. All power spectra and cospectra have a well-defined peak, which implies that the turbulent transport is not heavily affected by wake-induced turbulence caused by individual objects. Thus, the measurement height can be said to be high enough for turbulence caused by individual buildings to be blended together. The cospectral peaks in unstable stratification are close to observations from other urban and rural sites, and the peaks shift to higher frequencies as a function of stability, as expected. In contrast, low spectral values around $n/n_m = 0.3$, corresponding to scales of hundreds of metres, is evident for all cospectra and the u power spectrum but not for the w power spectrum. Elevated transport at low frequencies can be seen in the scalar cospectra, and the reason may be advection-induced large-scale circulations. Moreover, elevated transport at high frequencies can be seen in the momentum cospectrum: a slope of –1/3 (instead of –4/3) is evident in the inertial subrange at all sites; the inertial subrange slope of the sensible heat cospectrum also departs from predictions, with a –1 decay.

Though scalar similarity does not apply, and spectral intensities from the peak depart from their rural references, the EC method is applicable for urban sites where measurements are made above the roughness sublayer: the fluxes describe the dynamics of the surrounding area and common parametrizations, such as the logarithmic wind profile, apply. Special attention should be given, though, to the determination of roughness characteristics since they are the key to the convergence of international research on urban areas: a synthesis of urban studies can be made only with the aid of a clear framework based on dimensionless heights and reliable surface cover estimates. Furthermore, urban micrometeorology suffers from a lack of measurements for stable atmospheric stratification, a lack that is hindering the development of parametrizations under stable conditions.

Acknowledgments We acknowledge the support from the Academy of Finland through its Centre of Excellence program (Project No. 1118615, 138328), the ICOS project (No. 263149), and the EU-ICOS and EU-funded project BRIDGE. We would also like to thank Ivan Mammarella, Petri Keronen, Erkki Siivola and Üllar Rannik for their contributions to data acquisition and ideas. Hotel Torni and the Erottaja Fire Station are greatly acknowledged for providing the premises for the measurements. J.F.J. Korhonen is thanked for the photograph in Fig. 1d.

Appendix

Table 3 Fitting coefficients for integral turbulence characteristics (ITC) and cospectral peak frequency

	SMEAR III			Fire Station	Hotel Torni
	Built	Road	Vegetation		
Integral turbulence characteristics					
Unstable stratification ($\zeta < 0$)					
u	1.89, 0.16, 0.33	2.00, 0.33, 0.33	2.07, 0.30, 0.33	1.98, 0.27, 0.33	1.85, 0.09, 0.33
v	1.44, 1.04, 0.33	1.59, 1.21, 0.33	1.81, 1.42, 0.33	1.55, 1.17, 0.33	1.49, 0.41, 0.33
w	1.14, 1.88, 0.33	1.26, 1.40, 0.33	1.34, 1.28, 0.33	1.17, 1.23, 0.33	1.09, 1.20, 0.33
T	1.06, –, –0.33	1.22, –, –0.33	1.28, –, –0.33	1.15, –, –0.33	1.33, –, –0.33
c	3.35, 6.10, –0.33	2.72, 2.52, –0.33	3.04, 0.85, –0.33	4.15, 10.43, –0.33	2.75, 1.38, –0.33
q	1.94, 5.00, –0.33	2.34, 4.44, –0.33	2.02, 3.67, –0.33	8.39, 339.72, –0.33	2.57, 2.81, –0.33
Stable stratification ($\zeta > 0$)					
u	1.93, 0.97, 0.52	2.12, 5.09, 0.18	2.05, 2.08, 0.30	2.04, 0.91, 0.33	1.79, 1.20, 0.15
v	1.50, 2.86, 0.24	1.63, 9.39, 0.20	1.77, 1.70, 0.36	1.54, 3.12, 0.23	1.52, 0.26, 0.52
w	1.25, 1.38, 0.30	1.30, 8.09, 0.12	1.41, 1.53, 0.24	1.00, 583.41, 0.06	1.15, 2.19, 0.06
T	2.20, –, –0.21	1.27, –, –0.34	1.00, –, –0.42	1.01, –, –0.47	2.53, –, –0.32
c	2.36, –, –	2.66, –, –	2.37, –, –	3.30, –, –	3.03, –, –
q	1.93, –, –	2.72, –, –	2.16, –, –	3.35, –, –	2.47, –, –
Cospectral peak					
$\overline{w'u'}$		0.057, 4.042, 0.599		0.115, 2.118, 0.265	0.166, 2.346, 0.411
$\overline{w'T'}$		0.094, 4.355, 0.774		0.158, 0.783, 0.213	0.244, 1.589, 0.358
$\overline{w'q'}$		0.070, 3.352, 0.098		0.064, 2.048, 0.000	0.163, 2.628, 0.390
$\overline{w'c'}$		0.083, 3.864, 0.595		0.146, 1.831, 0.233	0.252, 1.352, 0.128

Coefficients for ITC are from Eqs. 1-3 (C_1, C_2, C_3), and values are given for along-wind (u), cross wind (v), vertical wind (w), temperature (T), CO_2 (c) and water vapour (q). Note that C_2 is not defined for T, the fits for $\zeta > 0$ did not succeed for water vapour and CO_2 (only mean values are given) and three land cover sectors are specified for SMEAR III. Coefficients for cospectral peak frequency as a function of stability $\left(n_{\mathrm{m}} = \alpha_1 \left(1 + \alpha_2 \zeta^{\alpha_3}\right)\right)$ are given for momentum ($\overline{w'u'}$), sensible heat ($\overline{w'T'}$), water vapour flux ($\overline{w'q'}$) and CO_2 flux ($\overline{w'c'}$)

References

Al-Jiboori MH, Xu YM, Qian YF (2002) Local similarity relationships in the urban boundary layer. Boundary-Layer Meteorol 102:63–82

Arnfield AJ (2003) Two decades of urban climate research: a review of turbulence, exchanges of energy and water, and the urban heat island. Int J Climatol 23:1–26. doi:10.1002/joc.859

Arya SP (2001) Introduction to micrometeorology. Academic Press, New York, 420 pp

Aubinet M, Grelle A, Ibrom A, Rannik Ü, Moncrieff J, Foken T, Kowalski AS, Martin PH, Berbigier P, Bernhofer C, Clement R, Elbers J, Granier A, Grunwald T, Morgenstern K, Pilegaard K, Rebmann C, Snijders W, Valentini R, Vesala T (2000) Estimates of the annual net carbon and water exchange of forests: the EUROFLUX methodology. Adv Ecol Res 30:113–175

Barlow JF, Harrison J, Robins AG, Wood CR (2011) A wind-tunnel study of flow distortion at a meteorological sensor on top of the BT tower, London, UK. J Wind Eng Ind Aerodyn 99:899–907

Burba GG, Mcdermitt DK, Anderson DJ, Furtaw MD, Eckles RD (2010) Novel design of an enclosed CO_2/H_2O gas analyser for eddy covariance flux measurements. Tellus Ser B 62:743–748. doi:10.1111/j.1600-0889.2010.00468.x

Cava D, Katul GG (2012) On the scaling laws of the velocity-scalar co-spectra in the canopy sublayer above tall forests. Boundary-Layer Meteorol (online first). doi:10.1007/s10546-012-9737-2

Christen A, Vogt R (2004) Energy and radiation balance of a central European city. Int J Climatol 24:1395–1421. doi:10.1002/joc.1074

Coutts AM, Beringer J, Tapper NJ (2007) Impact of increasing urban density on local climate: spatial and temporal variations in the surface energy balance in Melbourne, Australia. J Appl Meteorol Climatol 46:477–493. doi:10.1175/JAM2462.1

Drebs A, Nordlund A, Karlsson P, Helminen J, Rissanen P (2002) Tilastoja Suomen ilmastosta 1971–2000 [Climatological statistics of Finland 1971–2000]. Finnish Meteorological Institute, Helsinki

Foken T, Wichura B (1996) Tools for quality assessment of surface-based flux measurements. Agric For Meteorol 78:83–105

Foken T, Aubinet M, Leuning R (2012) The eddy covariance method. In: Aubinet M, Vesala T, Papale D (eds) Eddy covariance—a practical guide to measurement and data analysis. Springer Atmospheric Sciences, Dordrecht pp 1–19

Fortuniak K (2009) Selected characteristics of the atmospheric turbulence over a central European city centre—integral statistics. In: The seventh international conference on urban climate, 29 June–3 July 2009, Yokohama, Japan

Garratt JR (1992) The atmospheric boundary layer. Cambridge University Press, UK, 316 pp

Grimmond CSB, Oke TR (1999) Aerodynamic properties of urban areas derived, from analysis of surface form. J Appl Meteorol 38:1262–1292

Grimmond CSB, King TS, Cropley FD, Nowak DJ, Souch C (2002) Local-scale fluxes of carbon dioxide in urban environments: methodological challenges and results from Chicago. Environ Pollut 116:S243–S254. doi:10.1016/S0269-7491(01)00256-1

Grimmond CSB, Salmond JA, Oke TR, Offerle B, Lemonsu A (2004) Flux and turbulence measurements at a densely built-up site in Marseille: heat, mass (water and carbon dioxide), and momentum. J Geophys Res Atmos 109:D24101. doi:10.1029/2004JD004936

Hagishima A, Tanimoto J, Nagayama K, Meno S (2009) Aerodynamic parameters of regular arrays of rectangular blocks with various geometries. Boundary-Layer Meteorol 132:315–337. doi:10.1007/s10546-009-9403-5

Hanna SR, Zhou Y (2009) Space and time variations in turbulence during the Manhattan midtown 2005 field experiment. J Appl Meteorol Climatol 48:2295–2304. doi:10.1175/2009JAMC2046.1

Helfter C, Famulari D, Phillips GJ, Barlow JF, Wood CR, Grimmond CSB, Nemitz E (2011) Controls of carbon dioxide concentrations and fluxes above central London. Atmos Chem Phys 11: 1913–1928. doi:10.5194/acp-11-1913-2011

Hill RJ (1989) Implications of Monin–Obukhov similarity theory for scalar quantities. J Atmos Sci 46:2234–2244

HSY (2008) Seutu CD—a dataset by the Helsinki region environmental services authority

Järvi L, Mammarella I, Eugster W, Ibrom A, Siivola E, Dellwik E, Keronen P, Burba G, Vesala T (2009a) Comparison of net CO_2 fluxes measured with open- and closed-path infrared gas analyzers in an urban complex environment. Boreal Environ Res 14:499–514

Järvi L, Hannuniemi H, Hussein T, Junninen H, Aalto PP, Hillamo R, Mäkelä T, Keronen P, Siivola E, Vesala T, Kulmala M (2009b) The urban measurement station SMEAR III: continuous monitoring of air pollution and surface–atmosphere interactions in Helsinki, Finland. Boreal Environ Res 14:86–109

Järvi L, Nordbo A, Junninen H, Riikonen A, Moilanen J, Nikinmaa E, Vesala T (2012) Seasonal and annual variation of carbon dioxide surface fluxes in Helsinki, Finland, in 2006–2010. Atmos Chem Phys 12:8475–8489

Kaimal JC, Finnigan JJ (1994) Atmospheric boundary layer flows, their structure and measurements. Oxford University Press, New York, 289 pp

Kaimal JC, Izumi Y, Wyngaard JC, Cote R (1972) Spectral characteristics of surface-layer turbulence. Q J R Meteorol Soc 98:563–589

Kanda M, Moriwaki R, Kasamatsu F (2006) Spatial variability of both turbulent fluxes and temperature profiles in an urban roughness layer. Boundary-Layer Meteorol 121:339–350. doi:10.1007/s10546-006-9063-7

Katul G, Goltz S, Hsieh C, Cheng Y, Mowry F, Sigmon J (1995) Estimation of surface heat and momentum fluxes using the flux–variance method above uniform and nonuniform terrain. Boundary-Layer Meteorol 74:237–260. doi:10.1007/BF00712120

Kormann R, Meixner F (2001) An analytical footprint model for non-neutral stratification. Boundary-Layer Meteorol 99:207–224. doi:10.1023/A:1018991015119
Lenschow DH, Mann J, Kristensen L (1994) How long is long enough when measuring fluxes and other turbulence statistics. J Atmos Ocean Technol 11:661–673
Li QS, Zhi L, Hu F (2010) Boundary layer wind structure from observations on a 325 m tower. J Wind Eng Ind Aerodyn 98:818–832. doi:10.1016/j.jweia.2010.08.001
Lilleberg I, Hellman T (2011) The development of traffic in Helsinki in 2010 (in Finnish). Helsinki City Plann Dep 2:1–70
Liu HP, Peters G, Foken T (2001) New equations for sonic temperature variance and buoyancy heat flux with an omnidirectional sonic anemometer. Boundary-Layer Meteorol 100:459–468
Liu G, Sun J, Jiang W (2009) Observational verification of urban surface roughness parameters derived from morphological models. Meteorol Appl 16:205–213. doi:10.1002/met.109
MacDonald RW, Griffiths RF, Hall DJ (1998) An improved method for the estimation of surface roughness of obstacle arrays. Atmos Environ 32:1857–1864
McBean G (1970) The turbulent transfer mechanisms in the atmospheric surface layer. PhD thesis at the University of British Columbia
Metek (2006) USA-1 user manual, pp 1–55
Monin AS, Obukhov AM (1954) Dimensionless characteristics of turbulence in the surface layer. Akad Nauk SSR 24:163–187
Monin AS, Yaglom AM (1975) Statistical fluid mechanics. MIT Press, Cambridge, 875 pp
Moriwaki R, Kanda M (2006) Local and global similarity in turbulent transfer of heat, water vapour, and CO_2 in the dynamic convective sublayer over a suburban area. Boundary-Layer Meteorol 120:163–179. doi:10.1007/s10546-005-9034-4
Munger JW, Loescher HW, Luo H (2012) Measurement, tower, and site design considerations. In: Aubinet M, Vesala T, Papale D (eds) Eddy covariance—a practical guide to measurement and data analysis. Springer Atmospheric Sciences, Dordrecht pp 21–58
Nordbo A, Järvi L, Vesala T (2012) Revised eddy covariance flux calculation methodologies—effect on urban energy balance. Tellus Ser B 64:18184. doi:10.3402/tellusb.v64i0.18184
Oke TR (2006) Initial guidance to obtain representative meteorological observations at urban sites. In: Instrument and observing methods (IOM) 81. World Meteorological Organization, pp 1–51
Panofsky HA, Tennekes H, Lenschow DH, Wyngaard JC (1977) The characteristics of turbulent velocity components in the surface layer under convective conditions. Boundary-Layer Meteorol 11:355–361
Quan L, Hu F (2009) Relationship between turbulent flux and variance in the urban canopy. Meteorol Atmos Phys 104:29–36. doi:10.1007/s00703-008-0012-5
Rannik Ü (1998) On the surface layer similarity at a complex forest site. J Geophys Res Atmos 103:8685–8697. doi:10.1029/98JD00086
Rannik Ü, Vesala T (1999) Autoregressive filtering versus linear detrending in estimation of fluxes by the eddy covariance method. Boundary-Layer Meteorol 91:259–280
Rannik Ü, Keronen P, Hari P, Vesala T (2004) Estimation of forest-atmosphere CO_2 exchange by eddy covariance and profile techniques. Agric For Meteorol 126:141–155. doi:10.1016/j.agrformet.2004.06.010
Raupach MR (1979) Anomalies in flux–gradient relationships over forest. Boundary-Layer Meteorol 16:467–486
Roth M (2000) Review of atmospheric turbulence over cities. Q J R Meteorol Soc 126:941–990
Roth M, Oke TR (1995) Relative efficiencies of turbulent transfer of heat, mass, and momentum over a patchy urban surface. J Atmos Sci 52:1863–1874
Runkle BRK, Wille C, Gažovic M, Kutzbach L (2012) Attenuation correction procedures for water vapour fluxes from closed-path eddy-covariance systems. Boundary-Layer Meteorol 142(3):401–423. doi:10.1007/s10546-011-9689-y
Sofiev M, Genikhovich E, Keronen P, Vesala T (2010) Diagnosing the surface layer parameters for dispersion models within the meteorological-to-dispersion modeling interface. J Appl Meteorol Climatol 49:221–233. doi:10.1175/2009JAMC2210.1
Stone B, Hess JJ, Frumkin H (2010) Urban form and extreme heat events: are sprawling cities more vulnerable to climate change than compact cities?. Environ Health Perspect 118:1425–1428. doi:10.1289/ehp.0901879
Stull RB (1988) An introduction to boundary layer meteorology. Kluwer, Dordrecht, 666 pp
Tillman JE (1972) The indirect determination of stability, heat and momentum fluxes in the atmospheric boundary layer from simple scalar variables during dry unstable conditions. J Appl Meteorol 11:783–792
United Nations Population Division (2010) World urbanization prospects: the 2009 revision population database. http://esa.un.org/wup2009/unup/index.asp

van den Hurk BJJM, de Bruin HAR (1995) Fluctuations of the horizontal wind under unstable conditions. Boundary-Layer Meteorol 74:341–352

Velasco E, Roth M (2010) Cities as net sources of CO_2: review of atmospheric CO_2 exchange in urban environments measured by eddy covariance technique. Geogr Compass 4:1238–1259

Vesala T, Kljun N, Rannik Ü, Rinne J, Sogachev A, Markkanen T, Sabelfeld K, Foken T, Leclerc MY (2008a) Flux and concentration footprint modelling: state of the art. Environ Pollut 152:653–666. doi:10.1016/j.envpol.2007.06.070

Vesala T, Järvi L, Launiainen S, Sogachev A, Rannik Ü, Mammarella I, Siivola E, Keronen P, Rinne J, Riikonen A, Nikinmaa E (2008b) Surface–atmosphere interactions over complex urban terrain in Helsinki, Finland. Tellus Ser B 60:188–199. doi:10.1111/j.1600-0889.2007.00312.x

Vogt R, Christen A, Rotach MW, Roth M, Satyanarayana ANV (2006) Temporal dynamics of CO_2 fluxes and profiles over a central European city. Theor Appl Climatol 84:117–126. doi:10.1007/s00704-005-0149-9

Weaver H (1990) Temperature and humidity flux–variance relations determined by one-dimensional eddy-correlation. Boundary-Layer Meteorol 53:77–91. doi:10.1007/BF00122464

Webb EK, Pearman GI, Leuning R (1980) Correction of flux measurements for density effects due to heat and water-vapor transfer. Q J R Meteorol Soc 106:85–100

Weber S, Kordowski K (2010) Comparison of atmospheric turbulence characteristics and turbulent fluxes from two urban sites in Essen, Germany RID E-7434-2011. Theor Appl Climatol 102:61–74. doi:10.1007/s00704-009-0240-8

Wienhold FG, Frahm H, Harris GW (1994) Measurements of N_2O fluxes from fertilized grassland using a fast-response tunable diode-laser spectrometer. J Geophys Res Atmos 99:16557–16567

Wood CR, Arnold SJ, Balogun AA, Barlow JF, Belcher SE, Britter RE, Cheng H, Dobre A, Lingard JJN, Martin D, Neophytou MK, Petersson FK, Robins AG, Shallcross DE, Smalley RJ, Tate JE, Tomlin AS, White IR (2009) Dispersion experiments in central London—the 2007 Dapple project. Bull Am Meteorol Soc 90:955–970. doi:10.1175/2009BAMS2638.1

Wood CR, Lacser A, Barlow JF, Padhra A, Belcher SE, Nemitz E, Helfter C, Famulari D, Grimmond CSB (2010) Turbulent flow at 190 m height above London during 2006–2008: a climatology and the applicability of similarity theory. Boundary-Layer Meteorol 137:77–96. doi:10.1007/s10546-010-9516-xER

Wyngaard JC, Coté OR, Izumi Y (1971) Local free convection, similarity and the budgets of shear stress and heat flux. J Atmos Sci 28:1171–1182

Zilitinkevich SS, Mammarella I, Baklanov AA, Joffre SM (2008) The effect of stratification on the aerodynamic roughness length and displacement height. Boundary-Layer Meteorol 129:179–190. doi:10.1007/s10546-008-9307-9